RESEARCH ARTICLE | SEPTEMBER 13 2023

The significant magnetic attenuation with submicrometer scale magnetic phase separation in tensile-strained LaCoO$_3$ films

Yangyang Fan [ID] ; Xujing Li; Zhuo Yin; Aicong Geng [ID] ; Mengqin Wang [ID] ; Houbo Zhou [ID] ; Zheng Wang [ID] ; Xinchi Wang [ID] ; Jing Wang [✉] [ID] ; Fengxia Hu [✉] [ID] ; Baohe Li [✉] [ID] ; Jian-Tao Wang [✉] ; Baogen Shen [✉]

[Check for updates]
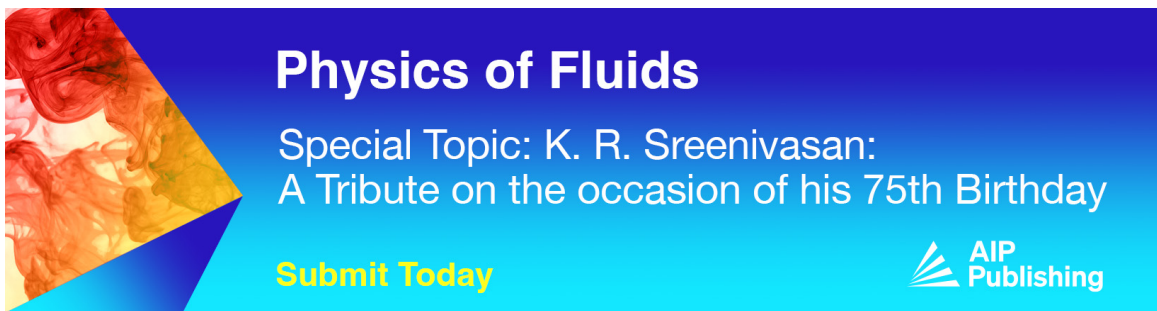
[ ] View Online   [ ] Export Citation   CrossMark

The significant magnetic attenuation with submicrometer scale magnetic phase separation in tensile-strained LaCoO₃ films

View Online　　Export Citation　　CrossMark

Yangyang Fan,[1,2] (iD) Xujing Li,[2] Zhuo Yin,[2,3] Aicong Geng,[1] (iD) Mengqin Wang,[2,3] (iD) Houbo Zhou,[2,3] (iD) Zheng Wang,[2,3] (iD) Xinchi Wang,[1] (iD) Jing Wang,[2,3,a)] (iD) Fengxia Hu,[2,3,4,a)] (iD) Baohe Li,[1,a)] (iD) Jian-Tao Wang,[2,3,a)] (iD) and Baogen Shen[2,3,5,a)]

AFFILIATIONS

[1] School of Physics, Beijing Technology and Business University, Beijing 100048, People's Republic of China
[2] Beijing National Laboratory for Condensed Matter Physics, Institute of Physics, Chinese Academy of Sciences, Beijing 100190, People's Republic of China
[3] School of Physical Sciences, University of Chinese Academy of Sciences, Beijing 101408, People's Republic of China
[4] Songshan Lake Materials Laboratory, Dongguan, Guangdong 523808, People's Republic of China
[5] Ningbo Institute of Materials Technology & Engineering, Chinese Academy of Sciences, 315201 Ningbo, Zhejiang, People's Republic of China

[a)]Authors to whom correspondence should be addressed: wangjing@iphy.ac.cn; fxhu@iphy.ac.cn; lbhe@th.btbu.edu.cn; wjt@iphy.ac.cn; and shenbg@iphy.ac.cn

ABSTRACT

It is well known that the epitaxial strain plays a vital role in tuning the magnetic states in transition metal oxide LaCoO₃ films. Here, we reported a robust long-range ferromagnetic (FM) ground state in a tensile-strained perovskite LaCoO₃ film on a SrTiO₃ (STO) substrate, which has a very significant attenuation when the thickness ranges from 10 to 50 nm. It is speculated that such attenuation may be caused by the appearance of the cross-hatched grain boundary, which relaxes the tensile strain around the crosshatch, resulting in the local non-FM phases. Magnetic force microscope observation reveals non-FM patterns correlated with the structural crosshatches in the strain-relaxed film even down to a temperature of 2 K and up to a magnetic field of 7 T, suggesting the phase separation origin of magnetization attenuation. Furthermore, the investigations of the temperature-dependent inverse magnetic susceptibility show a deviation from the Curie–Weiss law above the transition temperature in a 50-nm-thick LaCoO₃/STO film but not in the LaCoO₃/LaAlO₃ film, which is ascribed to the Griffiths phase due to the crosshatch-line grain boundaries. These results demonstrated that the local strain effect due to structural defects is important to affect the ferromagnetism in strain-engineered LaCoO₃ films, which may have potential implications for future oxide-based spintronics.

INTRODUCTION

The multivalent cations and strongly correlated d orbital electrons of transition metal oxides (TMOs) are responsible for a variety of physical characteristics, including metal–insulator transitions, superconductivity, magnetic ordering, ferroelectric polarization, and even magnetic phase separation.[1–3] It is well known that lattice strain plays a key role in determining the structure evolution and property optimization of TMOs with perovskite structures. Furthermore, strain engineering presents a promising route for creating novel physical phenomena, an exciting example is the recent demonstration of biaxial tensile strain tuning magnetism in cobaltites.[4–7] Perovskite cobaltite has attracted considerable attention due to its useful magnetic properties and novel physical behavior. Their intriguing physical properties are attributed to various spin states of cobalt ions determined by the delicate competition between Hund's exchange energy and crystal field splitting. Moreover, regulating the magnetism of cobalt ions is also useful for

an extensive range of technological applications, including batteries and solid-oxide fuel cells.[8–11] Therefore, studying the influence of lattice strain on its physical behavior is a positive sign for the realization of technological applications.

It has been reported that bulk perovskite LaCoO₃ (PV-LCO) exhibits a nonmagnetic insulator and low spin (LS) state at low temperatures, which transfers to an intermediate or high spin (IS or HS) state as the temperature increases, showing an interesting evolution of physical properties. Recent experiments have proved that the Co^{3+} ions in bulk exhibit a low spin state (LS, $t_{2g}^6 e_g^0$, $S = 0$) at the lowest temperature, which gradually changes to an intermediate spin state (IS, $t_{2g}^5 e_g^1$, $S = 1$) in a temperature range of 35 K < T < 100 K, and present a mixture of medium and high spin states (HS, $t_{2g}^4 e_g^2$, $S = 2$) in an interval of 300 K < T < 600 K, indicating the evolution of magnetic properties.[12–16] A particularly intriguing example is the observation of ferromagnetism in an epitaxial LaCoO₃ thin film, which provides a good platform to study strain-induced ground states in TMO thin films. It has been proposed that tensile strain is conducive to increasing the bandwidth of the energy band (e_g) and reducing the crystal field splitting effect (Δ_{CF}), which favors the occupation of the medium spin state and the high spin state. Numerous studies in theory and experimentation have attempted to explain the phenomena.[17–22] However, the microscopic origin of the ferromagnetic (FM) state is still not clear enough. Further research is still needed to fully understand the impact of local inhomogeneity on ferromagnetism in strained PV-LCO thin films.

Here, we conducted investigations into the combined effects of tensile and compressive strain on the magnetism in epitaxial LaCoO₃ thin films. High-quality epitaxial LaCoO₃ films have been grown on (001)-oriented SrTiO₃ (STO) and LaAlO₃ (LAO) substrates. Our results show that PV-LCO/STO thin films under tensile strain exhibit clearly long-range FM orders, whereas those under compressive strain exhibit only faint ferromagnetic behavior due to strain relaxation and defects. Furthermore, the magnetism of the 50-nm-thick PV-LCO/STO film has a very significant attenuation compared to the 10-nm-thick film, which is speculated to be the appearance of the cross-hatched grain boundary. In addition, the magnetic force microscope (MFM) experiments under high magnetic fields revealed crosshatch-correlated non-FM phases down to a measured temperature of 2 K in tensile-strained LaCoO₃ films, showing submicrometer-level magnetic phase separation. Meanwhile, in compressive-strained PV-LCO/LAO films of the same thickness, this phenomenon has not been seen. Furthermore, the measurements of the temperature-dependent inverse magnetic susceptibility show a non-linear temperature dependence and deviation from the Curie–Weiss law around the transition temperature in a 50-nm-thick LaCoO₃/STO film, indicating the existence of the Griffiths phase (GP) in the film containing local cross-hatched grain boundaries. Our findings provide new information for understanding the magnetic phase separation due to the local strain effect in strain-engineered LaCoO₃ films, which has positive significance for promoting the research and application of cobaltite thin films.

EXPERIMENTAL METHODS

In this work, the PV-LCO films were grown on single-crystalline substrates of STO and LAO, using pulsed-laser deposition (PLD). During deposition, a KrF excimer laser (λ = 248 nm) with a frequency of 2 Hz and a pulse energy of ~249 mJ was used to ablate the stoichiometric target. The LaCoO₃ target was prepared by the conventional solid reaction method. During the deposition, the oxygen pressure was kept at 30 Pa and the temperature of the substrate was kept at 700 °C. After deposition, the film was cooled down to room temperature at oxygen pressure (100 Pa). The surface morphology of PV-LCO films grown on STO and LAO substrates was investigated by using an atomic force microscope (AFM). The crystal structure of the films was measured by x-ray diffraction (XRD), and film thickness was determined using small-angle x-ray reflectivity (XRR). To better understand the structure, we compared reciprocal space mappings (RSMs) for films on STO and LAO substrates. The magnetic properties were characterized by measuring magnetic hysteresis loops, $M(H)$, and temperature-dependent magnetization, $M(T)$, via a superconducting quantum interference device vibrating sample magnetometer (SQUID-VSM). The magnetization saturation process of the film at 2 K was revealed using a magnetic force microscope (MFM) under a magnetic field as high as 7 T. To simulate the electronic and magnetic properties of LaCoO₃ films, first-principles calculations were performed on the tensile- and compressive-strained films, respectively, using the Vienna *ab initio* simulation package (VASP) with a distorted 2 × 2 × 2 supercell (see the supplementary material).

RESULTS AND DISCUSSION

The PV-LCO films grown on STO (mismatch = $a_{substrate} - a_{LCO}/a_{LCO}$) are under in-plane tensile strain, and films grown on LAO are under in-plane compressive strain, where a_{LCO} corresponds to the lattice parameters of the bulk LaCoO₃. The in-plane misfit strain of the LaCoO₃ films varies from −0.74% (compressive) to +2.17% (tensile) depending upon the substrate [Fig. 1(a)], which indicates that the substrate-induced misfit strain is accommodated by the elastic deformation of the films. Figure 1(b) shows the schematic crystal structures of the PV-LCO film and the STO/LAO substrate for a better understanding of the lattice matching, where the film was subjected to in-plane biaxial strain from the substrate.

In addition, XRD spectra were collected for the lattice planes parallel to the film plane. The XRD scans of PV-LCO films show symmetrical peak shapes and Laue fringes, indicating the good film crystalline quality of the films [Figs. 1(c)–1(e)]. The small angle x-ray reflectivity (XRR) measurements were performed to verify the thickness of LaCoO₃ by data fitting, and regular oscillation XRR results indicate the films have sharp interfaces and are highly crystalline [Fig. 2(b)]. From XRR fittings, the chemical depth profiles of those two films were obtained [Fig. 2(c)], and the x-ray scattering length density (SLD) directly indicates their uniform chemical distributions. Combined with the rocking curve of each LCO (002) reflection with a single peak shown in Fig. 2(d), good c-axis orientation can be further affirmed. To evaluate the crystallization quality of the films, the full width at half maximum (FWHM) of PV-LCO (002) diffraction peaks were measured from the rocking curves: 0.03° for LCO/STO and 0.17° for LCO/LAO. The small FWHM values in both films indicate a high degree of crystallinity for the PV-LCO films fabricated in our work. Note that the difference in FWHM between the two films may be due to the twins in the LAO substrate.
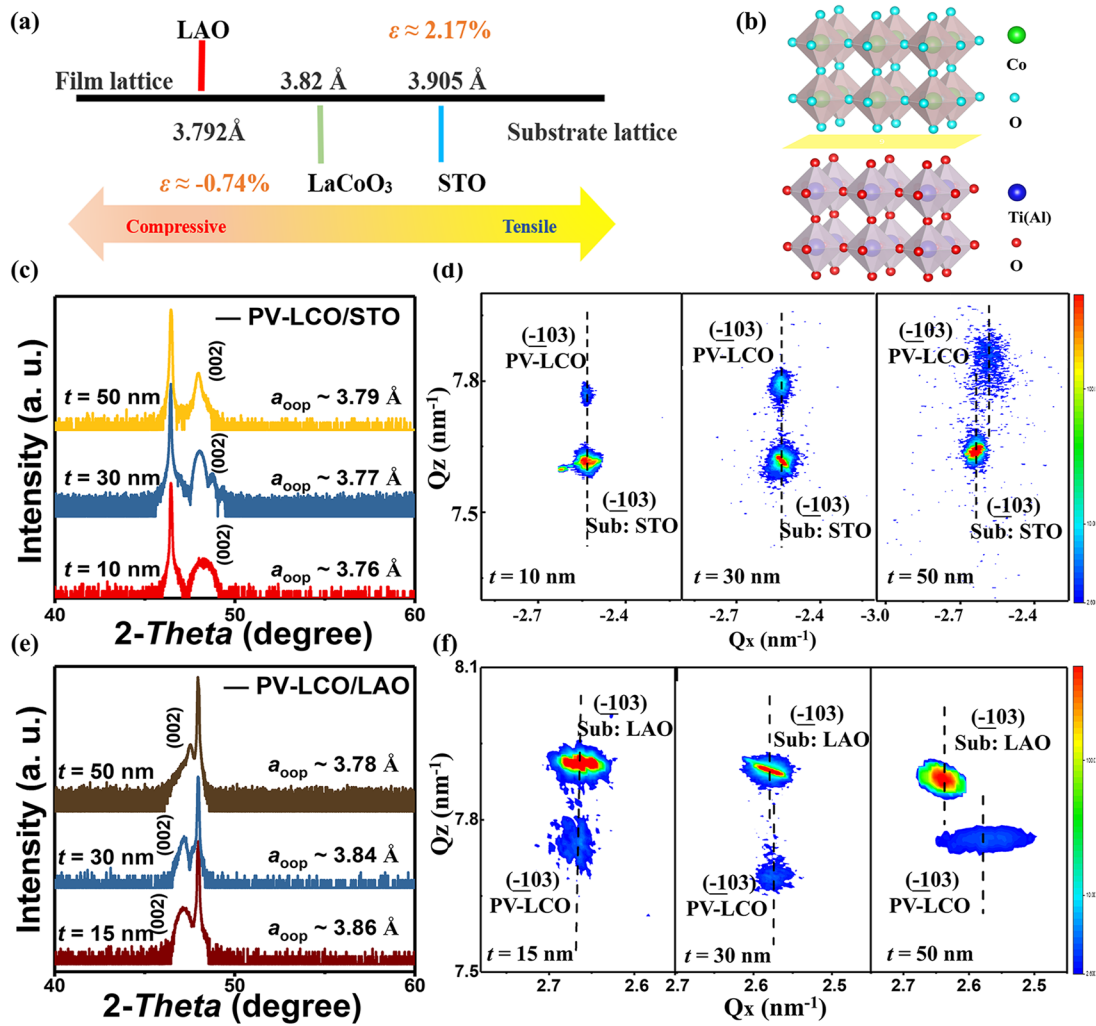
FIG. 1. (a) Lattice mismatch between the bulk perovskite LaCoO$_3$ and various substrates. (b) The crystal structures of PV-LCO film and STO/LAO substrate. (c) XRD θ-2θ scans of the PV-LCO films on the STO substrate. (d) Reciprocal space mappings of (-103) peak reflections for the PV-LCO/STO films. (e) XRD θ-2θ scans of the PV-LCO films on LAO substrate. (f) Reciprocal space mappings of (-103) peak reflections for the PV-LCO/LAO films.

The θ-2θ XRD measurements of the 002 peak [Fig. 1(c)] reveal that the strain clearly relaxes toward bulk LCO as a function of increasing thickness; the c-axis lattice parameters of PV-LCO/STO films are 3.76 Å for 10-nm-thick, 3.77 Å for 30-nm-thick, and 3.79 Å for 50-nm-thick, respectively. To better understand the overall structural changes as a function of thickness on STO, we compared reciprocal space maps taken at the (013) peaks for different thickness films [Fig. 1(d)]. RSMs show a weak strain relaxation phenomenon in the 50-nm-thick PV-LCO/STO film, which agrees with the observed variation of the θ-2θ XRD measurements and is in accordance with the previously reported Matthews–Blakeslee critical thickness for complete strain relaxation in LaCoO$_3$ films under tensile strain (~60 nm).[23–26] While for the films on LAO substrates, XRD spectra show that all the films are subjected to compressive

strain [Fig. 1(e)]. Meanwhile, an obvious compressive-strain relaxation phenomenon is observed in the 50-nm-thick PV-LCO/LAO film [Figs. 1(e) and 1(f)]. Furthermore, the surface morphology analysis of films grown on STO and LAO substrates was checked by atomic force microscopy. The surface roughness of rms was found to be ~3 Å, as shown in Fig. 2(a), indicating a smooth surface of all films. In summary, the structure and morphology characterizations of PV-LCO thin films are chemically uniform, highly crystalline, and single-phase. Meanwhile, images in Fig. 2(a) show some topographic lines with the crystallographic orientation on ⟨110⟩ in the 30-nm-thick PV-LCO/STO film, suggesting the appearance of cross-hatch-line grain boundaries that are probably related to local structural defects due to tensile strain relaxation.[27,28] This phenomenon is more pronounced in 50-nm-thick film, which
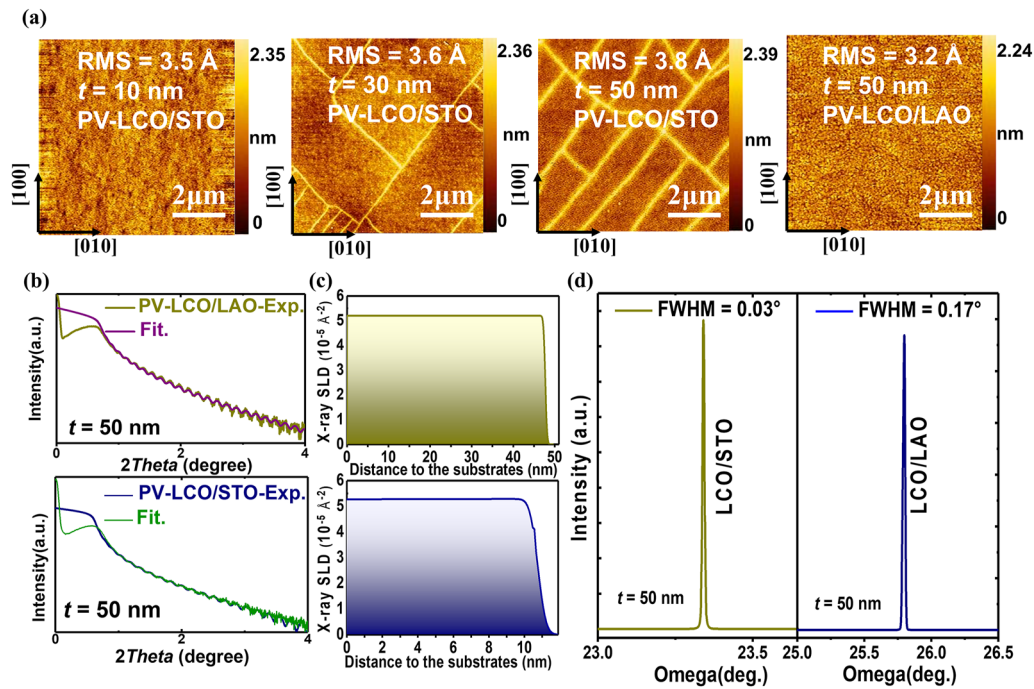
FIG. 2. (a) Surface morphology of the PV-LCO films on STO and LAO substrates. (b) XRR measurements and corresponding data fitting of LaCoO₃ films grown on STO and LAO substrates. (c) The chemical depth profiles from XRR fittings. (d) The rocking curves of the LCO (002) peak for the 50 nm films on STO and LAO substrates, respectively.

is similar to those observed in the previous report of the surface morphology in PV-LCO film with a thickness larger than 90 unit cells.[35]

This special morphologic phenomenon raises great interest in its impact on magnetic properties. To trace the variation of ferromagnetism, the temperature (T) and magnetic field (H) dependence of the magnetization (M) of PV-LCO films on STO substrates was measured and shown in Figs. 3(a) and 3(b), respectively. Apparent ferromagnetic behavior with an easy axis lying within the in-plane is observed in PV-LCO/STO films [Fig. 3(b)]. The spin state of Co ions is determined by the electronic configuration of the t_{2g} and e_g bands. It is believed that the tensile strain can increase the band length and promote the spin-state transition from the LS state to the IS or HS state due to the distortion and tilt of the CoO_6 octahedron (resulting in a decrease of Δ_{CF}), which favors the ferromagnetic double-exchange between occupied and unoccupied e_g orbitals. Our density functional theory (DFT) using the Vienna *ab initio* simulation package (VASP) calculations show that the Co 3d orbitals include two e_g and three t_{2g} orbitals on the LS site, while the energy level splits to four states (d_{xy}, d_{yz}/d_{xz}, d_{x2-y2}, and $d_z{}^2$) at the HS site tensile-strained LaCoO₃ film (supplementary material Fig. S1), resulting in the unoccupied e_g orbitals at LS site and half-occupied ones at neighboring HS site. This leads to the ferromagnetic double-exchange between neighboring Co ions and gives rise to ferromagnetism in the tensile-strained LaCoO₃ film.[28,35,41] The calculations also show that the LS and HS magnetic moments are 0.3 μ_B/Co and 2.9 μ_B/Co, respectively, leading to an average magnetic moment of 1.6 μ_B/Co, which matches well with the result of

1.3 μ_B/Co observed in our experiment. In addition, transport measurements demonstrated that all PV-LCO/STO films with different thicknesses exhibit insulating behavior [Fig. 3(c)],[29–32] which is also confirmed by the DFT calculations. Meanwhile, a substantial magnetism attenuation was observed in these PV-LCO/STO films. With the thickness increasing from 10 to 50 nm, the saturation magnetic moment decreases from 1.3 μ_B/Co to 0.7 μ_B/Co [see Fig. 3(b)]. This special magnetization attenuation may be related to the cross-hatched grain boundary emerging in the thicker film [Fig. 2(a)]. In our case, as the thickness of PV-LCO/STO films increases, the tensile strain from the lattice mismatch between the LaCoO₃ film and the STO substrate relaxes partially [see Fig. 1(d)], few available amounts of vacancies and local lattice distortions may lead to the appearance of a cross-hatched grain boundary and the FM regions coexisting with non-FM regions behaviors. As a result, the saturation magnetic moment of the film obviously attenuates with the increase in thickness.[35]

To further reveal the magnetic phase distribution in thin films, the magnetization saturation process of the 50-nm-thick PV-LCO/STO film was investigated by using a low-temperature magnetic force microscope. Obvious evidence of FM regions coexisting with non-FM regions is observed. The MFM images were recorded during the field increase after zero-field cooling. The different colors in the MFM images show different interactions between the tip and the local area. Since the MFM tip is only sensitive to the out-of-plane magnetization, the green color represents negligible interactions from non-FM regions, and spin-up and spin-down states are represented by red and blue colors (Fig. 4), respectively. As shown in Fig. 4(a), the obvious-separated FM droplets dipped into weak/non-
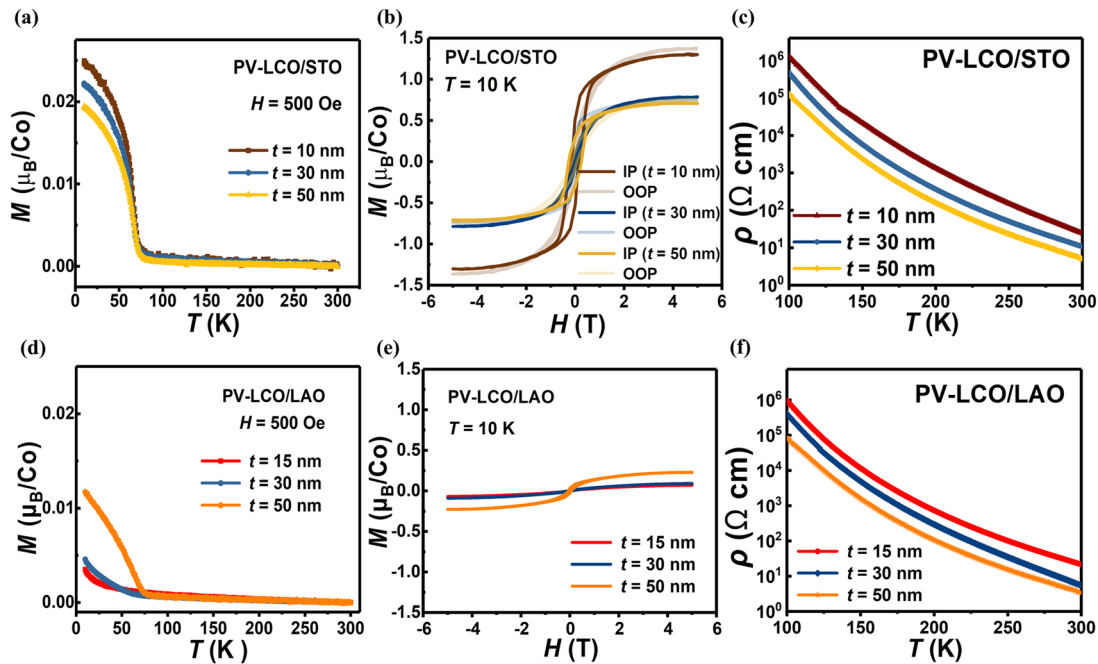
FIG. 3. (a) Temperature dependence of magnetization $M(T)$ for the PV-LCO/STO films under field cooling, measured by applying an in-plane magnetic field $H = 500$ Oe. (b) In-plane (IP) and out-of-plane (OOP) magnetic hysteresis loops for the PV-LCO/STO films measured at 10 K. (c) Resistivity of the PV-LCO/STO films as a function of temperature. (d) M–T curves of the PV-LCO/LAO films under field cooling. (e) M–H curves of the PV-LCO/LAO films at 10 K. (f) Resistivity of the PV-LCO/LAO films as a function of temperature.

FM regions. The FM droplets gradually expand [Figs. 4(b)–4(e)] with the field increasing. When the field exceeds 4 T, the size of the observed FM regions remains almost unchanged. Even when the magnetic field reaches 7 T, the FM area still cannot completely fill the entire area. As no exchange bias phenomenon was found in the magnetization measurements [Fig. 3(b)], one can exclude the possibility of coexisting antiferromagnetism. Thus, this non-FM

phase could be paramagnetic or diamagnetic since LaCoO$_3$ has a very abundant magnetic phase diagram in the bulk.[33–35] Moreover, one can find that the patterns, especially in images under a low magnetic field, have a clear orientation of $\langle 110 \rangle$, which correlates with the topographic crosshatch feature [see Fig. 2(a)]. This strong correlation between the surface morphology result and the MFM of the 50-nm LCO/STO film suggests that the observed magnetic
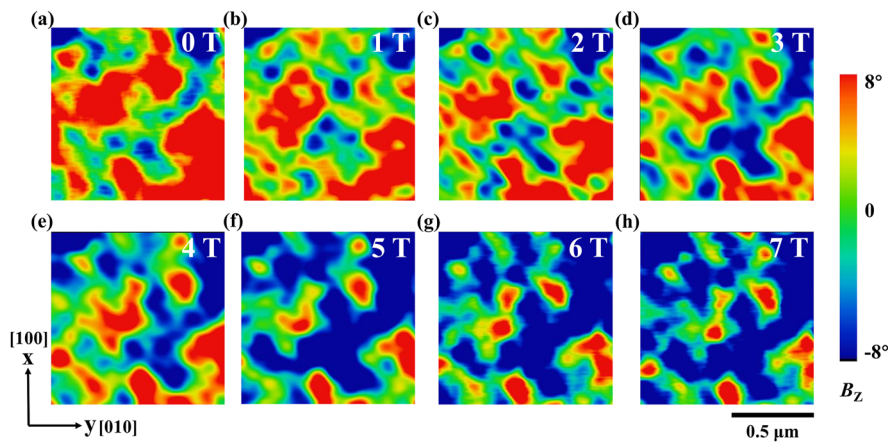
FIG. 4. Magnetic force microscopy investigations on 50-nm-thick PV-LCO film. (a)–(h) Representative MFM images measured at 2 K and taken with increasing field. All images were taken in the same area after zero-field cooling. For all images, the scanning area is 1×1 μm^2. The color bar is $\pm 8°$ for phase shift.

phase separation is caused by the cross-hatched grain boundaries in thick films, further confirming that the magnetization attenuation in thick films originates from the local structural defects. These defects, including local vacancies, lattice distortion, and misfit dislocations, can effectively release the tensile strain, resulting in the non-FM regions.

Interestingly, it was found that this local structural defect not only results in magnetic phase separation but also affects the magnetic behavior near the magnetic transition. Figures 5(a)–5(c) show the temperature dependence of the inverse magnetic susceptibility, χ^{-1}, for tensile-strained PV-LCO/STO films. A liner temperature dependence of χ^{-1} in the temperature region higher than Curie temperature is observed for 10-nm-thick LCO/STO film [Fig. 5(a)], in good correspondence with the Curie–Weiss law. Whereas the obvious non-linear temperature dependence of χ^{-1} above the Curie temperature emerges as increasing the thickness of LCO/STO films. In particular, for the 50-nm LCO/STO film, a downward deviation from Curie's law was observed. It has been reported that local short-range FM order could occur in the temperature range $T_G > T > T_C$, due to the random disorder resulting in Griffiths singularity,[36,37] where T_G is the intrinsic ordering temperature in the system free of disorder. In our case, the possible sources of disorders may be small amounts of vacancies and local lattice distortions near the cross-hatched grain boundaries.[35]

According to the Griffiths phase (GP) model, the GP singularity is defined as a non-linear T-dependence for the $\chi^{-1}(T)$ in the low field by the following equation:[38]

$$\chi^{-1} \propto \left(T - T_C{}^R\right)^{1-\lambda}, \qquad (1)$$

where $T_C{}^R$ is the random ferromagnetic transition temperature in the clusters, $0 < \lambda < 1$ is the exponent characterizing the strength of GP, and λ is supposed to be zero in the pure PM area. Based on this Griffiths phase mode, we fitted the curves of temperature-dependent $\chi^{-1}(T)$ for 10, 30, and 50-nm LCO/STO films, and the results are shown in Figs. 5(a)–5(c). Obviously, the deviation from the Curie–Weiss law is found in the 30 and 50-nm thick LaCoO$_3$ films on STO, indicating that the short-range FM clusters exist in the PM region, and the simulated strength index (λ) of Griffiths phase is equal to 0.27 for the 50-nm thick LaCoO$_3$ film.

Furthermore, we have also undertaken a comparative study of the epitaxial tensile and compressive strain on the magnetic and transport properties of PV-LCO thin films. Similar to LCO/STO films, all PV-LCO/LAO films also exhibit insulating behavior [see Fig. 3(f)]. Unlike the PV-LCO/STO film, 15 and 30-nm thick films strained on LAO substrates do not show ferromagnetic hysteresis [see Figs. 3(d) and 3(e)], which agree that the epitaxial compressive strain does not give rise to ferromagnetism.[35] However, the 50-nm-thick PV-LCO/LAO film exhibits very weak ferromagnetism [Fig. 3(e)]. Meanwhile, a good agreement with the Curie–Weiss law and no sign of the Griffiths phase is observed for the 50-nm-thick LaCoO$_3$ film on LAO [Fig. 5(d)]. Furthermore, the magnetization saturation process of the 50-nm-thick PV-LCO/LAO film was investigated by using a low-temperature magnetic force microscope, and no obvious magnetic contrast was observed, even down to a lowest
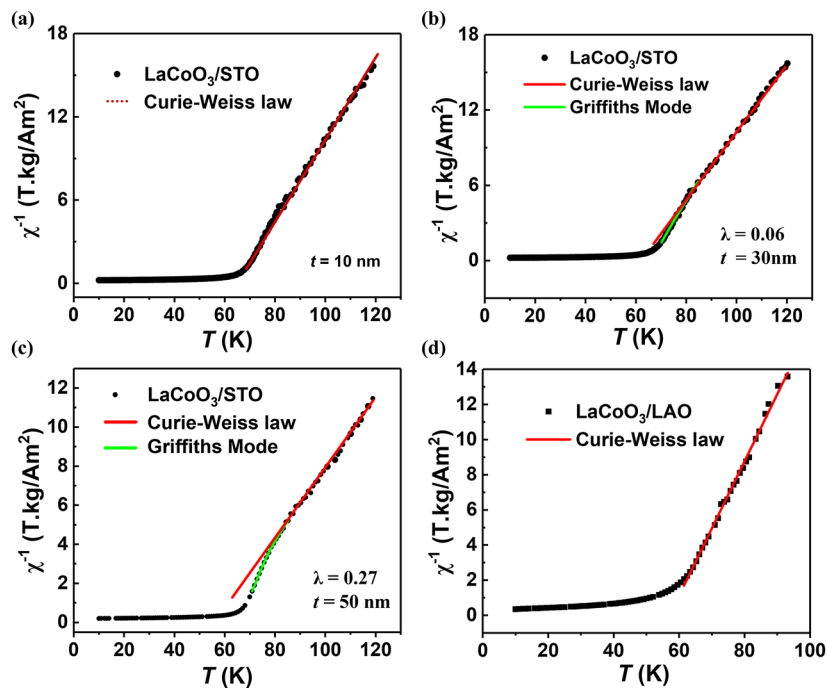
FIG. 5. (a)–(d) The plots of χ^{-1} vs T for PV-LCO films on STO and LAO substrates, respectively. The red line corresponds to fitting by the Curie–Weiss law, and the green line is fitting using the Griffith phase model.

temperature of 2 K and up to a magnetic field of 7 T. DFT calculations show that the t_{2g} orbital is split into a higher singlet d_{xy} and a lower doublet (d_{zx} and d_{yz}), and e_g orbitals are split into two separate energy levels d_z^2 and d_{x2-y2} at the IS state due to the Jahn–Teller distortion and octahedral tilt by compressive strain. Thus, there is a relatively large population of e_g electrons at the IS state, leading to a weak ferromagnetic exchange interaction between neighboring LS and IS Co ions. Meanwhile, the calculations show that the mix LS–IS states are metastable with higher energy, which makes the fully compressive-strained PV-LCO/LAO films (15 and 30 nm) favor the nonmagnetic state with the suppression of the transition between LS and IS states, as shown in Fig. 3(e). Whereas, the lattice relaxation in the 50 nm-thick PV-LCO/LAO film [Fig. 1(f)] decreases the tetragonal distortion in a way and, thus, introduces oxygen vacancies in the lattice.[39] This lattice relaxation, together with the oxygen vacancy, may work synergistically to lower the energy and stabilize the IS state,[40] leading to the weak ferromagnetism observed in 50-nm-thick PV-LCO/LAO film.[41–44]

CONCLUSION

In summary, high-quality LaCoO₃ epitaxial thin films were successfully grown on STO and LAO substrates by PLD. Our experiments showed that PV-LCO/STO films exhibit strong ferromagnetism, while thin PV-LCO/LAO films (15, 30 nm) are nonmagnetic despite that a very weak ferromagnetic behavior appears in the 50-nm thick film due to the lattice relaxation and the total number of defects. The first-principles calculations indicate that the ferromagnetism in tensile-strained films is ascribed to the exchange interaction between LS- and HS-Co ions that is induced by the distortion and tilt of the CoO₆ octahedron, further emphasizing the crucial role of tensile strain in inducing ferromagnetism in LaCoO₃ films. In addition, the weak ferromagnetism in the 50 nm PV-LCO/LAO film may come from the synergy of lattice relaxation and oxygen vacancies. Moreover, the saturation magnetic moment of the 30 and 50-nm tensile-strained films shows a significant attenuation compared to the 10-nm-thick LaCoO₃ film, which is ascribed to the cross-hatch-line grain boundaries appearing in the thicker films. The obvious evidence of FM regions coexisting with non-FM regions is observed by MFM, even if the magnetic field reaches 7 T. The strong correlation between the surface morphology result and MFM of the 50-nm-thick LCO/STO film further confirms that the magnetization attenuation in thicker films originates from the local cross-hatched grain boundaries. In addition, an obvious deviation from the Curie–Weiss law is found in the 50-nm-thick LaCoO₃ films on STO substrate, which is caused by the presence of the Griffiths phase due to the cross-hatched grain boundary. Our findings provide valuable information into the origin of the magnetic phase separation in strain-engineered LaCoO₃ films, which has the potential to promote the application of perovskite structural-functional oxide devices.

SUPPLEMENTARY MATERIAL

The supplementary material file gives the first-principles calculation using the Vienna *ab initio* simulation package (VASP).

AUTHOR DECLARATIONS

Conflict of Interest

The authors have no conflicts to disclose.

Author Contributions

J. Wang and F. X. Hu conceived the idea and designed the experiments, B. G. Shen supervised the research. Others participated in the discussion and analysis.

Y. Y. Fan: Investigation (lead); Methodology (equal); Writing – original draft (lead). **X. J. Li**: Methodology (equal). **Z. Yin**: Investigation (equal); Methodology (equal). **A. C. Geng**: Methodology (equal). **M. Q. Wang**: Methodology (equal). **H. B. Zhou**: Methodology (equal). **Z. Wang**: Investigation (equal). **X. C. Wang**: Investigation (equal). **J. Wang**: Conceptualization (lead); Funding acquisition (equal); Methodology (lead); Writing – review & editing (lead). **F. X. Hu**: Conceptualization (equal); Funding acquisition (equal); Writing – review & editing (equal). **B. H. Li**: Writing – review & editing (equal). **J.-T. Wang**: Methodology (equal); Writing – review & editing (equal). **B. G. Shen**: Funding acquisition (equal); Writing – review & editing (equal).

DATA AVAILABILITY

The data that support the findings of this study are available within the article.

REFERENCES

[1] J. A. Bert, B. Kalisky, C. Bell, M. Kim, Y. Hikita, H. Y. Hwang, and K. A. Moler, Nat. Phys. **7**, 767 (2011).

[2] M. Gibert, P. Zubko, R. Scherwitzl, J. Iniguez, and J. M. Triscone, Nat. Mater. **11**, 195 (2012).

[3] L. Li, C. Richter, J. Mannhart, and R. C. Ashoori, Nat. Phys. **7**, 762 (2011).

[4] Y. Zhu, Y. Fu, B. Tu, T. Li, J. Miao, Q. Zhao, S. Wu, J. Xia, P. Zhou, A. Huq, W. Schmidt, D. Ouyang, Z. Tang, Z. He, and H.-F. Li, Phys. Rev. Mater. **4**, 094409 (2020).

[5] S. Smadici, P. Abbamonte, A. Bhattacharya, X. Zhai, B. Jiang, A. Rusydi, J. N. Eckstein, S. D. Bader, and J.-M. Zuo, Phys. Rev. Lett. **99**, 196404 (2007).

[6] M. W. Haverkort, Z. Hu, J. C. Cezar, T. Burnus, H. Hartmann, M. Reuther, C. Zobel, T. Lorenz, A. Tanaka, N. B. Brookes, H. H. Hsieh, H. J. Lin, C. T. Chen, and L. H. Tjeng, Phys. Rev. Lett. **97**, 176405 (2006).

[7] J. Fujioka, Y. Yamasaki, H. Nakao, R. Kumai, Y. Murakami, M. Nakamura, M. Kawasaki, and Y. Tokura, Phys. Rev. Lett. **111**, 027206 (2013).

[8] J. Li, M. X. Guan, P. F. Nan, Jing. Wang, B. H. Ge, K. M. Qiao, H. R. Zhang, W. H. Liang, J. Z. Hao, H. B. Zhou, F. R. Shen, F. X. Liang, C. Zhang, M. Liu, S. Meng, T.

04 December 2023 02:05:16

Zhu, F. X Hu, T. Wu, J. D. Guo, J. R. Sun, and B. G. Shen, Nano Engry. **78**, 105215 (2020).

[9] J. S. White, M. Bator, Y. Hu, H. Luetkens, J. Stahn, S. Capelli, S. Das, M. Dobeli, Th. Lippert, V. K. Malik, J. Martynczuk, A. Wokaun, M. Kenzelmann, Ch. Niedermayer, and C. W. Schneider, Phys. Rev. Lett. **111**, 037201 (2013).

[10] O. H. Hansteen, H. Fjellvag, and B. C. Hauback, J. Solid State Chem. **141**, 411 (1998).

[11] D. V. Christensen, Y. Frenkel,, Y. Z. Chen, Y. W. Xie, Z. Y. Chen, Y. Hikita, A. Smith, L. Klein, H. Y. Hwang, N. Pryds, and B. Kalisky, Nat. Phys. **15**, 269–274 (2019).

[12] D. W. Jeong, W. S. Choi, S. Okamoto, J. Y. Kim, K. W. Kim, S. J. Moon, D. Y. Cho, H. N. Lee, and T. W. Noh, Sci. Rep. **4**, 6124 (2014).

[13] D. Fuchs, C. Pinta, T. Schwarz, P. Schweiss, P. Nagel, S. Schuppler, R. Schneider, M. Merz, G. Roth, and H. v. Löhneysen, Phys. Rev. B **75**(14), 144402 (2007).

[14] P. L. Kuhns, M. J. R. Hoch, W. G. Moulton, A. P. Reyes, J. Wu, and C. Leighton, Phys. Rev. Lett. **91**, 127202 (2003).

[15] J. W. Freeland, J. X. Ma, and J. Shi, Appl. Phys. Lett. **93**(21), 212501 (2008).

[16] J. R. Petrie, C. Mitra, H. Jeen, W. S. Choi, T. L. Meyer, F. A. Reboredo, J. W. Freeland, G. Eres, and H. N. Lee, Adv. Funct. Mater. **26**, 1564–1570 (2016).

[17] H. Seo, A. Posadas, and A. A. Demkov, Phys. Rev. B **86**(1), 014430 (2012).

[18] B. Kalisky, J. A. Bert, B. B. Klopfer, C. Bell, H. K. Sato, M. Hosoda, Y. Hikita, H. Y. Hwang, and K. A. Moler, Nat. Commun. **3**, 922 (2012).

[19] J. Zhang, Z. Zhong, X. Guan, X. Shen, J. Zhang, F. Han, H. Zhang, H. Zhang, X. Yan, Q. Zhang, L. Gu, F. Hu, R. Yu, B. Shen, and J. Sun, Nat. Commun. **9**, 1923 (2018).

[20] G. Araizi-Kanoutas, J. Geessinck, N. Gauquelin, S. Smit, X. H. Verbeek, S. K. Mishra, P. Bencok, C. Schlueter, T.-L. Lee, D. Krishnan, J. Fatermans, J. Verbeeck, G. Rijnders, G. Koster, and M. S. Golden, Phys. Rev. Mater. **4**, 026001 (2020).

[21] Y. Zhu, K. Du, J. Niu, L. Lin, W. Wei, H. Liu, H. Lin, K. Zhang, T. Yang, Y. Kou, J. Shao, X. Gao, X. Xu, X. Wu, S. Dong, L. Yin, and J. Shen, Nat. Commun. **7**, 11260 (2016).

[22] H. Zhou, L. Wang, Y. Hou, Z. Huang, Q. Lu, and W. Wu, Nat. Commun. **6**, 8980 (2015).

[23] V. V. Mehta, N. Biskup, C. Jenkins, E. Arenholz, M. Varela, and Y. Suzuki, Phys. Rev. B **91**, 144418 (2015).

[24] J. M. Rondinelli, and R. M. Spaldin, Phys. Rev. B. **79**, 054409 (2009).

[25] P. E. Vullum, R. Holmestad, H. L. Lein, J. Mastin, M.-A. Einarsrud, and T. Grande, Adv. Mater. **19**, 4399 (2007).

[26] P. E. Vullum, H. L. Lein, M.-A. Einarsrud, T. Grande, and R. Holmestad, Philos. Mag. **88**, 1187 (2008).

[27] S. Park, P. Ryan, E. Karapetrova, J. W. Kim, J. X. Ma, J. Shi, J. W. Freeland, and W. Wu, Appl. Phys. Lett. **95**, 072508 (2009).

[28] Z.-H. Wang, O. I. Lebedev, G. Van Tendeloo, G. Cristiani, and H.-U. Habermeier, Phys. Rev. B **77**, 115330 (2008).

[29] F. Golmar, A. M. M. Navarro, C. E. R. Torres, F. H. Sánchez, F. D. Saccone, P. C. dos Santos Claro, G. A. Benítez, and P. L. Schilardi, Appl. Phys. Lett. **92**, 262503 (2008).

[30] S. Zhou, L. Shi, J. Zhao, L. He, H. Yang, and S. Zhang, Phys. Rev. B **76**, 172407 (2007).

[31] Q. Lu and B. Yildiz, Nano Lett. **16**, 1186–1193 (2016).

[32] Q. Zhang, A. Gao, F. Meng, Q. Jin, S. Lin, X. Wang, D. Xiao, C. Wang, K.-j. Jin, D. Su, E. J. Guo, and L. Gu, Nat. Commun. **12**, 1853 (2021).

[33] T. Raoufi, A. G. Varzaneh, M. H. Ehsani, E. Liu, and V. Chernenko, Mater. Res. Bull. **156**, 111997 (2022).

[34] M. A. Torija, M. Sharma, J. Gazquez, M. Varela, C. He, J. Schmitt, J. A. Borchers, M. Laver, S. El-Khatib, and C. Leighton, Adv. Mater. **23**, 2711 (2011).

[35] Q. Y. Feng, D. C. Meng, H. B. Zhou, G. H. Liang, Z. Z. Cui, H. L. Huang, J. L. Wang, J. H. Guo, C. Ma, X. Zhai, Q. Lu, and Y. Lu, Phys. Rev. Mater. **3**, 074406 (2019).

[36] C. Chen, J. Avila, E. Frantzeskakis, A. Levy, and M. C. Asensio, Nat. Commun. **6**, 8585 (2015).

[37] R. B. Griffiths, Phys. Rev. Lett. **23**, 17 (1969).

[38] M. Mukesh, B. Arun, V. Akshay, and M. Vasundhara, New J. Chem. **44**(31), 13480–13487 (2020).

[39] N. B. Zhang, X. H. Tian, Y. L. Zhu, Y. J. Wang, Y. L. Tang, M. J. Zou, J. Y. Ma, Y. P. Feng, W. R. Geng, Y. Cao, and X. L. Ma, J. Phys. Chem. C **124**(23), 12492–12501 (2020).

[40] N. Biškup, J. Salafranca, V. Mehta, M. P. Oxley, Y. Suzuki, S. J. Pennycook, S. T. Pantelides, and M. Varela, Phys. Rev. Lett. **112**(8), 087202 (2014).

[41] C. F. Chang, Z. Hu, H. Wu, T. Burnus, N. Hollmann, M. Benomar, T. Lorenz, A. Tanaka, H.-J. Lin, H. H. Hsieh, C. T. Chen, and L. H. Tjeng, Phys. Rev. Lett. **102**, 116401 (2009).

[42] S. I. Csiszar, M. W. Haverkort, Z. Hu, A. Tanaka, H. H. Hsieh, H.-J. Lin, C. T. Chen, T. Hibma, and L. H. Tjeng, Phys. Rev. Lett. **95**, 187205 (2005).

[43] H. Seo, A. Posadas, and A. A. Demkov, Phys. Rev. B **86**, 014430 (2012).

[44] J. Gazquez, S. Bose, M. Sharma, M. A. Torija, S. J. Pennycook, C. Leighton, and M. Varela, APL Mater. **1**, 012105 (2013).